Infrared analogs of heteronuclear nuclear magnetic resonance coherence transfer experiments in peptides

C. Scheurer[a] and S. Mukamel[b]
Department of Chemistry, University of Rochester, Rochester, New York 14627

Using short pulses whose bandwidth covers only one amide band and that are resonant with either the amide I or the amide II band, we propose two-color multiple pulse infrared experiments that are analogs of heteronuclear nuclear magnetic resonance (NMR) experiments for probing the structure of peptides and proteins. These pulse sequences yield simpler spectra of nonoverlapping vibrational bands with fewer overlapping peaks than one-color techniques, and open new ways to more sophisticated control over coherence transfer pathways. Differences between NMR and IR techniques stemming from the different initial conditions and the pulse field strengths are taken into account. We find that in several cases, π pulses commonly used in NMR to simplify the spectra can be avoided in vibrational spectroscopy due to the low temperature initial condition (i.e., vibrational energies are large compared to kT). © *2002 American Institute of Physics.*
[DOI: 10.1063/1.1461362]

I. INTRODUCTION

The vibrational spectrum of a macromolecule built from a set of similar repetitive units contains bands that can be described in terms of vibrations localized at these units and their couplings between. These vibrational bands can be modeled by a Frenkel exciton Hamiltonian.[1–5] The couplings as well as the transition frequencies of the localized oscillators depend on the molecular geometry and typically yield broad unresolved bands in absorption (one-dimensional) experiments. The spectroscopic resolution can be increased considerably and some of the geometric and dynamic information can be recovered using multidimensional techniques.[6–19] Pulsed ultrafast vibrational spectroscopy has many analogies to nuclear magnetic resonance (NMR).[20–22] Historically, multidimensional NMR started with simple pulse sequences applied to small molecules.[23–25] Much more elaborate techniques have subsequently been developed for complex molecules with thousands of atoms.[26–28] Multidimensional vibrational spectroscopy stands at the beginning of a similar development.

Recently, one-color IR techniques analogous to important homonuclear NMR experiments have been identified.[21] To study large molecules it is necessary to increase the resolution and to simplify the spectra even further than in these simple experiments. This can be achieved making use of frequency resolution during specific time intervals in a multidimensional pulse sequence and is the basis of heteronuclear NMR, which is of great importance for studying structure and dynamics of complex molecules like peptides and proteins.[26–28] The frequency resolution is not used to select individual chromophores but rather to separate different isotopic species or, in infrared spectroscopy, different vibrational bands. Multicolor multidimensional IR experiments can potentially yield more detailed information on the vibrational motions in polypeptides and achieve higher resolutions than one-color experiments, in analogy to heteronuclear NMR. At the same time these time-domain (rather than frequency-domain) measurements offer high temporal resolution due to the large pulse bandwidth and short pulse duration needed to cover a whole vibrational band.

A prerequisite for multicolor IR analogs of heteronuclear NMR experiments is the existence of several spectrally well resolved but rather broad and intense vibrational bands. Proteins contain bands of peptide plane modes above 1400 cm^{-1} with strong transition dipole moments.[29,30] These bands are usually denoted the amide-A, amide-B, amide-II, and the amide-I band (see Fig. 1). All of these modes which are spectrally well separated from the remaining bands have been studied extensively in small peptides as well as using *N*-methylacetamide (NMA) as a model.[29,31]

The vibrational 1600–1700 cm^{-1} amide-I band has been widely studied by ordinary one-dimensional IR spectroscopy[32] and is the subject of most multidimensional IR spectroscopical studies of peptides and proteins conducted so far. This mode has a strong transition dipole moment and is clearly distinguishable from other vibrational modes of the amino acid residues (see Fig. 1). An early study of model peptides made of a single type of amino acids[29] demonstrated that the coupling between CO stretching modes in different peptide bonds is due to transition dipole coupling which results in a delocalization of the amide-I states and can be described by a Frenkel exciton model.[33] The dependence of the dipole–dipole coupling on the relative orientations and distances of the interacting dipoles yields an amide-I band signature of the three-dimensional structure of the protein.

The different secondary structure elements occurring in proteins result in characteristic amide-I signatures which form the basis of polypeptide and protein structure

[a]Electronic mail: chris@feynman.chem.rochester.edu
[b]Electronic mail: mukamel@chem.rochester.edu
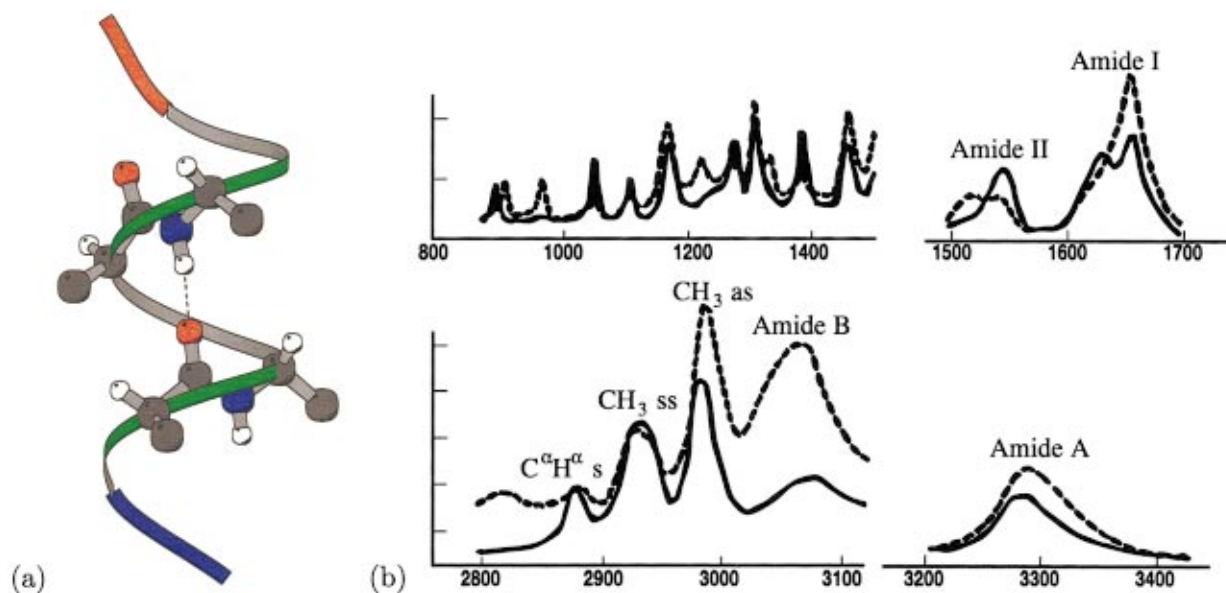
FIG. 1. (Color) (a) Structure of a ten-residue α-poly(L-alanine), showing a hydrogen bonded pair of peptide planes with indices $(i, i+3)$. (b) IR spectra in the midinfrared region ($800-3400$ cm^{-1}) with the electric vector perpendicular (full line) or parallel (dashed line) to the direction of orientation.

determinations.[34,35] The complicated three-dimensional structure of proteins leads to overlapping bands corresponding to these different secondary structural elements. These bands are additionally inhomogeneously broadened by conformational fluctuations of the secondary structure and by coupling to the local solvent environment, yielding a highly congested amide-I band and calling for sophisticated pulse techniques to gain the necessary resolution to study larger molecules. The amide-II modes are only weakly coupled to the amide-I band (transition energy differences ~ 100 cm^{-1} and couplings <10 cm^{-1}). Localized peptide plane vibrations of the nonoverlapping amide-I and amide-II bands can assume the role of the different nuclear species in heteronuclear NMR experiments. In analogy to the corresponding NMR experiments (e.g., heteronuclear multiple quantum correlation) it should be possible to address individual peptide planes by correlating vibrations at different frequencies through couplings within a single peptide plane. It might also be possible to select pairs of peptide planes by their characteristic couplings through hydrogen bonds, e.g., in α helices or β sheets, in analogy to the very recent NMR studies of trans-hydrogen bond J couplings.[36–41]

In this paper we propose several vibrational analogs of simple heteronuclear NMR techniques. In Sec. II we describe the vibrational exciton Hamiltonian for the amide-I and amide-II bands and discuss the spectral features of coupling mechanisms that are common to liquid state NMR and vibrational spectroscopy. The choice of Hamiltonian parameters, as explained in Sec. IV, was made in order to best illustrate all possible peaks. The focus of this paper is on the question of which principles can be transferred from NMR spectroscopy and how the spectra and pulse sequences differ from NMR due to the major differences such as the low temperature and weak pulse field limits. To gain this insight we used parameters that allow the resolution of all peaks and a detailed analysis of the spectra in terms of the coherence trans-

fer pathways. More quantitative simulations using a recently developed exciton Hamiltonian for the protein amide bands which is based on a classical protein force field will be presented in the future.[42]

The pulse sequences for vibrational analogs of simple heteronuclear NMR experiments are introduced in Sec. III. We devise the vibrational techniques by analogy with the NMR sequences, building upon our recent analysis of the spectroscopy of coupled two-level systems which provides rules for mapping strong field NMR pulse sequences into weak field IR.[21,22] The main features of the new spectroscopic techniques are discussed in detail for a small model system in Sec. IV. All spectra are calculated using the operator propagation expressions (26) of Ref. 21. Relaxation is only taken into account with a simple model of homogeneous broadening. Since our main focus is on understanding the coherence transfer pathways that contribute to the spectra we will not discuss effects of inhomogeneous broadening. The molecular dynamics (MD) simulation of inhomogeneously broadened spectra is an ongoing project.[5,42]

II. THE VIBRATIONAL EXCITON HAMILTONIAN

We consider a molecule whose vibrational modes consist of a set of coupled localized anharmonic oscillators described by the following zero order Hamiltonian,[42]

$$H_0 = \sum_{mn} U_u^m B_m^\dagger B_n + \sum_{mnkl} U_{kl}^{mn} B_m^\dagger B_n^\dagger B_k B_l, \quad (1)$$

where we retained only terms up to fourth order that preserve the number of excitons. The operators $B_m^\dagger$, B_n are boson creation and annihilation operators for the localized vibrations that fulfill the boson commutation relations

$$[B_m, B_n^\dagger] = \delta_{mn}, \quad (2)$$

which determines the specific dependence, introduced by normal ordering, of the U_n^m matrix elements in Eq. (1) on the fourth-order derivatives of the potential energy surface. A similar Hamiltonian was used previously to describe electronic and vibrational Frenkel excitons in molecular aggregates and proteins.[43,44] That Hamiltonian was expressed using different, non-Boson operators. The collective vibrational modes obtained by diagonalizing the first term of Eq. (1) are denoted vibrational excitons, and Eq. (1) is the vibrational exciton Hamiltonian. Here and in the following we distinguish between parameters of the exciton Hamiltonian (e.g., U_{mn}, U_{nkl}^m) to different orders by the numbers of superscripts (subscripts) denoting indices related to creation (annihilation) operators.

The terms in the Hamiltonian up to fourth order that either create or destroy one vibrational exciton are given by

$$H' = \sum_m U_m(B_m + B_m^\dagger) + \sum_{mnk} U_{nk}^m(B_m^\dagger B_n B_k + B_n^\dagger B_k^\dagger B_m). \tag{3}$$

The vibrational response functions for fifth-order Raman experiments based on a perturbative treatment of the vibrational Hamiltonian containing the second sum in Eq. (3) have recently been derived using an equations of motion approach.[45] A similar Hamiltonian was used with $U_{nk}^m = U_{nn}^m \delta_{nk}$ to describe the energy transport along chains of hydrogen bonded peptides in an α-helical peptide[46] where the third-order term in Eq. (3) accounted for the 2:1 Fermi resonance coupling between the amide-I band and the NH stretch vibration of the amide-A,B bands.

The most important interchromophore couplings in vibrational and NMR spectroscopy are described by *off-diagonal* second-order terms $U_j^i B_i^\dagger B_j + \text{c.c.}$ and *diagonal* fourth-order terms $U_{ij}^{ij} B_i^\dagger B_j^\dagger B_i B_j + \text{c.c.}$ The former coupling elements are known as excitonic coupling in optical spectroscopy or strong J coupling in NMR ($I_{x,i}I_{x,j} + I_{y,i}I_{y,j}$). The fourth-order coupling is an anharmonic contribution in vibrational spectroscopy (Darling–Dennison coupling[47]) and corresponds to the weak coupling case of NMR ($I_{z,i}I_{z,j}$). Coupled chromophores with negative (positive) off-diagonal electronic coupling are known as J aggregates (H aggregates). The two have very different fluorescence spectra and quantum yields.[48]

Including the coupling with the radiation field, the total Hamiltonian has the form

$$H_T = H_0 + H' - \mathcal{E}(t)\boldsymbol{\mu}, \tag{4}$$

where $\boldsymbol{\mu}$ is the vibrational transition dipole in the electronic ground state, which depends on the vibrational coordinates. The transition dipole moment may be expanded in terms of the coordinates as was done for the potential energy. To third order we have

$$\boldsymbol{\mu} = \sum_n (D_n B_n + D^n B_n^\dagger) + \sum_{mn} (D_{mn} B_m B_n + D^{mn} B_m^\dagger B_n^\dagger$$
$$+ D_n^m B_m^\dagger B_n) + \sum_{mkl} (D_{kl}^m B_m^\dagger B_k B_l + D_m^{kl} B_k^\dagger B_l^\dagger B_m), \tag{5}$$

where the $D_{l_1 \cdots l_n}^{k_1 \cdots k_m}$ are vectorial expansion coefficients and we have retained all terms that create or annihilate up to two excitons. The terms in the second and third sum of Eq. (5) constitute vibrational nonlinearities that have different spectroscopic signatures than those in the potential energy operator.[22,49]

The coupling to the electric field $\mathcal{E}(t)\boldsymbol{\mu}$ can be expressed in analogy to the potential energy terms with matrix elements

$$E_{l_1 \cdots l_n}^{k_1 \cdots k_m}(t) \equiv \mathcal{E}(t) \cdot D_{l_1 \cdots l_n}^{k_1 \cdots k_m}, \tag{6}$$

which are time dependent due to the field $\mathcal{E}(t)$. The field-dependent contribution to the total Hamiltonian then becomes

$$\mathcal{E}(t)\boldsymbol{\mu} = \sum_n (E_n(t)B_n + E^n(t)B_n^\dagger) + \sum_{mn} (E_{mn}(t)B_m B_n$$
$$+ E^{mn}(t)B_m^\dagger B_n^\dagger + E_n^m(t)B_m^\dagger B_n)$$
$$+ \sum_{mkl} (E_{kl}^m(t)B_m^\dagger B_k B_l + E_m^{kl}(t)B_k^\dagger B_l^\dagger B_m). \tag{7}$$

For experiments involving multiple separated pulses, the $D_{l_1 \cdots l_n}^{k_1 \cdots k_m}$ are tensorial elements that depend on the polarization of the individual pulses. These elements should be averaged over the rotational distribution of the molecules in the sample and the choice of pulse polarizations provides additional control parameters which allow one to simplify the resulting spectra considerably.[50–52] All of the exciton Hamiltonian parameters may be computed using quantum chemistry codes. This will allow first principles simulations of realistic multidimensional spectra. In this paper we retain those terms that are essential for the optical response and use the resulting simplified Hamiltonian (see Sec. IV) to explore possible pulse sequences.

III. HETERONUCLEAR NMR PULSE SEQUENCES AND THEIR MULTICOLOR INFRARED COUNTERPARTS

Heteronuclear pulse sequences which use a specific heteronuclear coherence transfer to considerably simplify the spectra are of great importance in multidimensional NMR studies of complicated molecules such as biopolymers.[26–28] This transfer requires a coupling J between the different spin species, and the delays t' in the transfer sequence can be chosen to maximize transfer for certain pairs of spins connected with a coupling of a specified magnitude. The resulting spectrum will then ideally only contain peaks corresponding to pairs fulfilling the transfer condition $t' = 1/(2J)$.[27] This can be used to obtain information about the bonding topology in a molecule, which is the basis of the sequential NMR protein assignment techniques.[26,28] Once each peak is assigned to a specific site, it is possible to use this information in more complicated relaxation experiments to obtain data about molecular structure and dynamics. This additional information is frequently obtained by heteronuclear methods that contain the simpler coherence transfer schemes as building blocks that provide simplified well-resolved spectra.[53] To that end additional delays are introduced in the pulse sequence during which auto- and cross-

relaxation is active and a series of two-dimensional (2D) spectra is recorded. The variation of the peak intensities with the relaxation period can be described theoretically with models for the relaxation active coupling mechanism, like dipolar or (chemical shift anisotropy) interactions, and spectral density functions for the bath.[54–57] Structural parameters are obtained, for example, from the strong distance dependence of the dipolar cross relaxation (NOE), and dynamical time scales and order parameters can be extracted from the time-dependent peak intensities.

Another use of heteronuclear coherence transfer in more elaborate pulse sequences is the indirect observation of transitions with small dipole moments through their coupling to transitions with strong dipole moment as in INEPT (insensitive nuclei enhanced by polarization transfer).[27] This technique is frequently used to enhance the sensitivity of carbon or nitrogen spectroscopy [which is low due to the small gyromagnetic ratios of ^{13}C and ^{15}N, see Eq. (9)] by coherence transfer from protons. It is then possible to manipulate the coherences of the less sensitive spins and finally either detect them directly or transfer the coherence back to the more sensitive species for detection. In this section we present third- and fifth-order vibrational analogs of heteronuclear NMR coherence transfer experiments (Figs. 2 and 3) which are closely related to INEPT (Fig. 4).[27] We also discuss third- and fifth-order analogs of the heteronuclear multiple quantum correlation (HMQC) experiment (Fig. 5).[28] These techniques are by themselves important 2D NMR experiments but furthermore constitute frequently used building blocks in more elaborate pulse schemes. We will first discuss the most important concepts underlying the NMR pulse sequences. Despite the differences in the Hamiltonians (which will be discussed in the following) many of these concepts are transferable and allow us to devise analogous IR pulse sequences. We present both NMR and IR techniques using a model of two frequency bands A and B. In heteronuclear NMR these bands are traditionally named the I (insensitive) and S (sensitive) spins. For IR spectroscopy of peptides they represent, for example, the amide-I and amide-II bands.

All NMR two-color coherence transfer experiments require a coupling between chromophores in bands A and B that produces $A-B$ correlated density matrix elements.[27] The off-resonant coupling between chromophores belonging to bands A and B in two-color experiments can be described in analogy to the weak J-coupling limit in NMR provided it is much smaller than the difference in transition frequencies of bands A and B. Our exciton Hamiltonian also contains the resonant coupling term which yields additional contributions but the main features of the spectroscopic technique can be understood based on the weak coupling approximation in which the coupling is described by an $I_{z,A}I_{z,B}$ operator term in NMR or corresponding fourth-order terms of the form $B_A^\dagger B_B^\dagger B_A B_B + \text{c.c.}$ in the normal-ordered exciton Hamiltonian, respectively.

We will discuss the pulse sequences in terms of coupled two-level systems which simplifies the comparison with NMR. The liquid state NMR Hamiltonian for which the following experiments were designed consists of the Zeeman
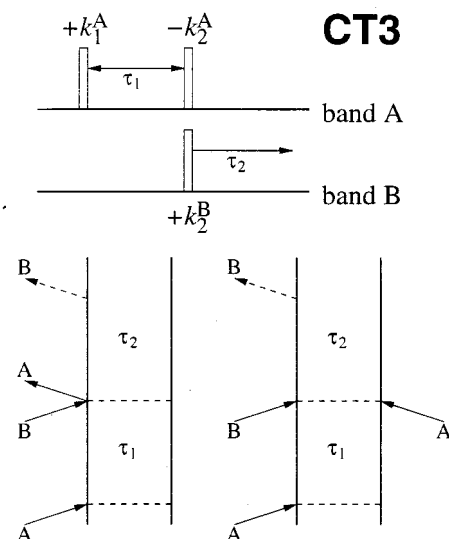
FIG. 2. The simplest two-color coherence transfer experiment using three pulses. The open bars represent $\pi/2$ pulses in NMR. The corresponding wave vectors for weak field IR spectroscopy are given next to the bars. The Feynman diagrams show the coherence transfer pathways involved in the response of the system.

term, the isotropic coupling term, and the coupling to the external field $\mathcal{E}(t)$[27,58,59]

$$H^{\text{NMR}} = \sum_i^N \omega_i I_{z,i} + \sum_{i<j}^N J_{ij}(I_{x,i}I_{x,j} + I_{y,i}I_{y,j} + I_{z,i}I_{z,j})$$
$$- \mathcal{E}(t)\boldsymbol{\mu}, \qquad (8)$$

where the dipole is determined by the gyromagnetic ratio for the isotopic species γ_I and the spin operators

$$\boldsymbol{\mu} = \gamma_I \vec{I}. \qquad (9)$$

The generalization to vibrational multilevel systems introduces additional peaks that contain further information about anharmonicities but preserve the key features of the pulse sequences.[21]

The vertical bars in Figs. 2–5 represent pulses resonant with the transitions of the respective bands, as indicated. For NMR pulse sequences the closed bars represent π pulses and the open bars $\pi/2$ pulses. In the case of weak-field IR the open bars denote a single interaction with a pulse with the wave vector indicated next to the bar, while the closed bars correspond to the interaction with two correctly phased time-coincident pulses which perform a transformation of the density matrix yielding a signal that is closely related to the π-pulse transformation if observed in the correctly phase matched direction. The transformation of the density matrix under the action of such pulse pairs yields the closest analog of a NMR π pulse for coupled two-level systems.[21]

The basic NMR heteronuclear coherence transfer scheme (CT3) consists of a single pulse on band A, followed by two coincident pulses (one resonant with band A and the other with band B, see Fig. 2).[27] The first pulse creates a one-quantum coherence of the A chromophores. The coupling between the A and B chromophores then leads to the formation of an $A-B$ correlated state during the period τ_1.
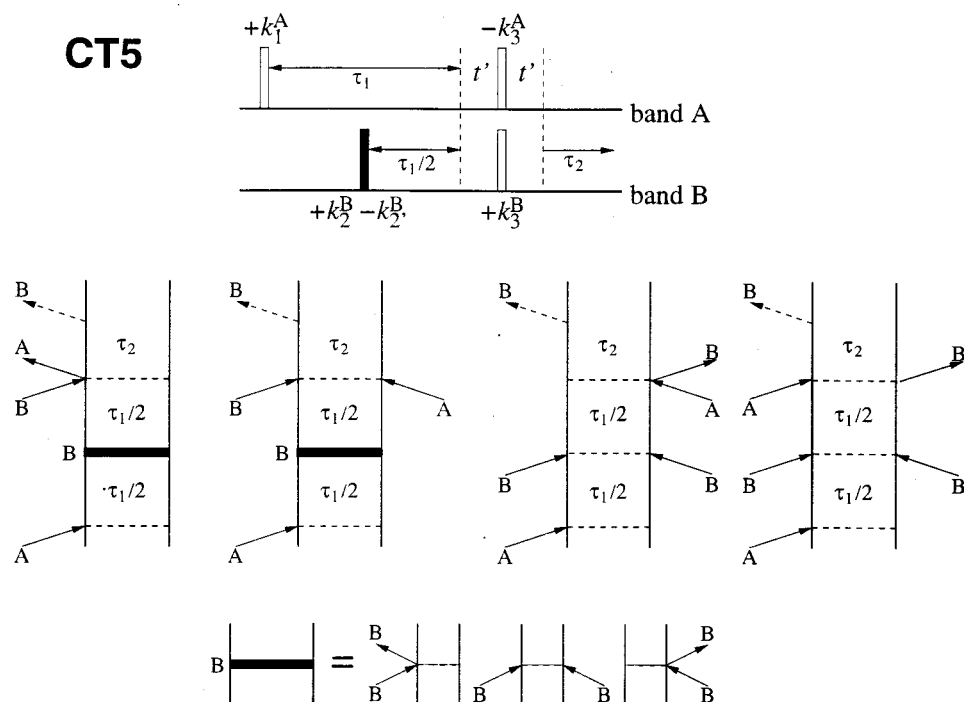
FIG. 3. Fifth-order frequency correlation experiment. The closed bars represent π pulses in NMR and the open bars $\pi/2$ pulses. The corresponding wave vectors for weak field IR spectroscopy are given next to the bars.

The two coincident pulses perform a transfer of the coherence from A to B. It is not necessary for the transfer that the two pulses $\mathbf{k}_2^A$ and $\mathbf{k}_2^B$ be phase coherent.[27] This is well known in NMR and can be seen from the Feynman diagrams, since the coherence is converted into a phase independent correlated $A-B$ population state by the pulse $\mathbf{k}_2^A$ which is subsequently transferred into a coherence of the B chromophores. The two coincident pulses can therefore be
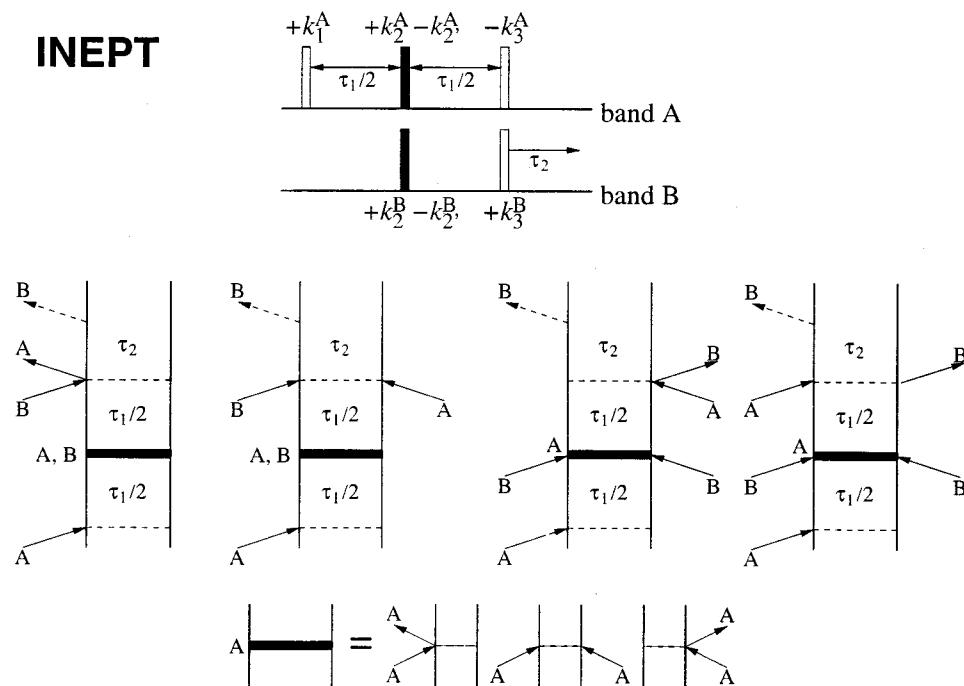
FIG. 4. The INEPT experiment. The closed bars represent π pulses in NMR and the open bars $\pi/2$ pulses. The corresponding wave vectors for weak field IR spectroscopy are given next to the bars.
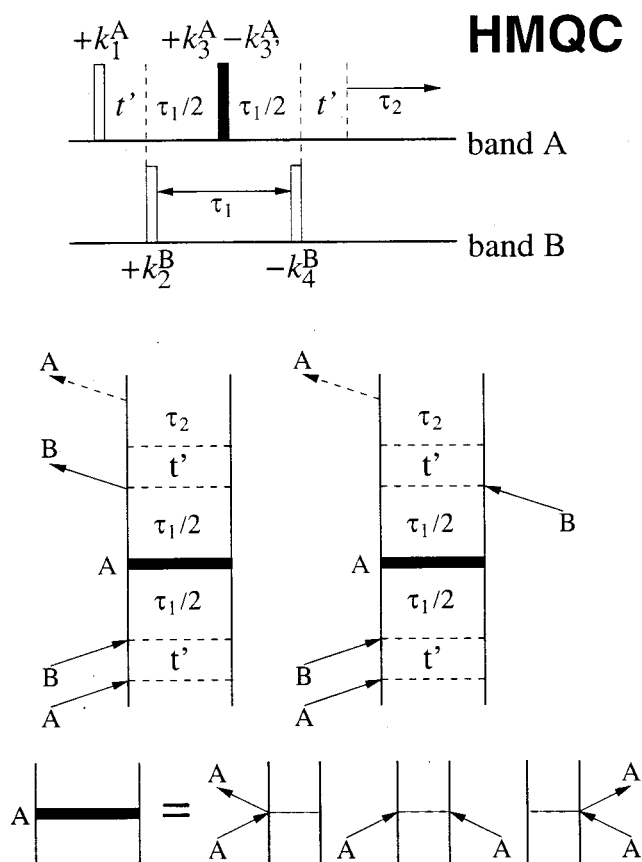
FIG. 5. The HMQC experiment. The closed bars represent π pulses in NMR and the open bars $\pi/2$ pulses. The corresponding wave vectors for weak field IR spectroscopy are given next to the bars. The modified vibrational experiment HMQC' does not contain the $\mathbf{k}_3$ pulse pair on the A band. The Feynman diagrams show the coherence transfer pathways involved in the response of the system.

either derived from a single pulse with a bandwidth that covers both bands or from two independent pulses. The experiment is two-dimensional with domains given by the delay times τ_1 and τ_2 and is third order with respect to the laser fields. This simple experiment demonstrates the possibility of pulse induced coherence transfer between coupled chromophores but is otherwise not widely used in NMR since the evolution in both time domains is under the full Hamiltonian which results in complicated spectra.

It is possible to derive several pulse schemes that remedy this problem by introducing additional pulses and delays to better control the evolution of coherences.[27] The introduction of a π pulse on the B band in the center of the delay τ_1, for example, refocuses the B band evolution as well as the $A-B$ coupling, yielding an effective evolution under the A band Hamiltonian alone during τ_1 (CT5, see Fig. 3). It is then necessary to introduce a delay t' before and after the coincident A and B pulses to obtain a correlated state for the coherence transfer by the pulse pair. This delay can be adjusted to optimize transfer through specific couplings. The system then evolves under the combined Hamiltonian during τ_2. Broadband decoupling, i.e., irradiation with a strong resonant radio-frequency field,[27,59] of the A band is often applied in NMR during τ_2, yielding an effective evolution

under the B band Hamiltonian alone for this time domain. The resulting technique is known as ''shift correlation spectroscopy'' since chemical shift evolution of the A band during τ_1 is correlated with chemical shift evolution of the B band during τ_2 by coherence transfer via an $A-B$ coupling. Broadband decoupling is not possible for weak field IR techniques, making the spectra somewhat more complex in the Ω_2 direction. However if the couplings within a single band are unresolved, the information content of the spectra is the same as in ''shift correlation spectroscopy'' and contains peaks only from $A-B$ pairs of chromophores connected by a coupling that has the correct magnitude compared to t'.

The important INEPT sequence (see Fig. 4) can also be derived from the general correlation scheme.[27] The introduction of coincident π pulses on both bands in the center between the $\pi/2$ pulses of Fig. 2 refocuses the evolution within the A band and within the B band but preserves the evolution of the $A-B$ coupling which is necessary for the creation of the correlated state used for the coherence transfer. The delay τ_1 can be chosen to maximize the transfer for specific groups of coupled chromophores. The π pulses are substituted by pulse pairs $+\mathbf{k}_2^A-\mathbf{k}_{2'}^A$, and $+\mathbf{k}_2^B-\mathbf{k}_{2'}^B$, in the analogous IR experiment which yields an echo response at time $2\tau_1$ similar to the refocussing used in NMR. The resulting technique is seventh order in the fields.

All the above mentioned pulse sequences only generate populations and single quantum coherences. It is also possible to create higher order coherences in heterosystems and use combinations of transitions to obtain frequency correlation maps. For example, this is the idea of the HMQC pulse sequence given in Fig. 5.[28] The first pulse creates a coherence of the A chromophores which evolves during the delay t' into an $A-B$ correlated state due to the coupling J connecting chromophores belonging to the different bands. The fixed delay t' can be adjusted to maximize the coherence transfer through a specific coupling by choosing t' $=1/(2J)$. The second pulse transfers the correlated state into a double quantum coherence that evolves during τ_1 with a sum frequency of the order of $\Omega_A+\Omega_B$. The central π pulse refocuses both the free (noncoupled) evolution of A chromophores and the couplings between the A and the B band during the time $2t'+\tau_1$. The last pulse transfers the double quantum coherence back to an observable polarization. In the direct vibrational analog, the central NMR π pulse is substituted by two time coincident pulses on band A. The resulting experiment is fifth order in the fields and two-dimensional with respect to the τ_1 and τ_2 time domains. This pulse sequence does not produce any observable signal for band B alone, and the experiment looks like a heterodyne detected one-color reverse transient grating experiment ($\mathbf{k}_1+\mathbf{k}_2$ $-\mathbf{k}_{2'}$)[44] if only band A is considered. The multiple quantum coherence transfer yields a modulation of the signal of band A with the double quantum frequencies, which can be observed. We shall also consider a modified pulse sequence HMQC' obtained by deleting the $\mathbf{k}_3$ pulses.

IV. APPLICATION TO THE AMIDE BANDS OF PEPTIDES

In this section we discuss the signals expected for the pulse sequences introduced in Sec. III for the amide-I and amide-II bands in proteins and peptides. We shall use a simplified model Hamiltonian with $N=4$ chromophores (two belonging to the amide-I band and two are in the amide-II band). The corresponding transition frequencies are chosen as $\omega_1 = 1530 \text{ cm}^{-1}$, $\omega_2 = 1560 \text{ cm}^{-1}$, $\omega_3 = 1620 \text{ cm}^{-1}$, and $\omega_4 = 1650 \text{ cm}^{-1}$, which are typical for peptide spectra.[29] We assume that chromophores one and three are from one peptide plane while chromophores two and four belong to a neighboring plane. Additionally we take the same anharmonicity of $\Delta = -16 \text{ cm}^{-1}$ for all modes (this value has been found experimentally for amide-I vibrations[60]). The coupling topology is depicted in Fig. 8. The coupling between chromophores in a single band is treated as an excitonic, off-diagonal coupling with coupling operator $J_{ij} B_i^\dagger B_j$ and the size of the matrix elements J_{ij} is chosen in agreement with the transition dipole coupling model of the amide-I band for neighboring peptide planes in a peptide chain.[29,33] We use $J_{12} = -5 \text{ cm}^{-1}$ and $J_{34} = 5 \text{ cm}^{-1}$, while all other matrix elements are zero since for these couplings the transition frequency differences are large compared to the coupling matrix elements and can be neglected. For the interband coupling terms we only retain the nonresonant diagonal contributions $K_{ij}/2 B_i^\dagger B_j^\dagger B_i B_j$, which are equivalent to the weak coupling observed in liquid state NMR [second term in Eq. (8)]. Based on calculations of anharmonic coupling terms from a classical MD force field,[42] we use $K_{13} = 8 \text{ cm}^{-1}$ and $K_{24} = 16 \text{ cm}^{-1}$ to describe the coupling between amide-I and amide-II chromophores within the same peptide plane (coupling between mainly CO and CN stretch vibrations) and neglect all anharmonic couplings between chromophores in different peptide planes. These rather large couplings were chosen in order to better resolve all peaks and allow a qualitative analysis of the coupling patterns. More quantitative calculations with smaller, more realistic, couplings and microscopic modeling of line broadening will be presented elsewhere.[42]

The zero-order model Hamiltonian is of the general form of Eq. (1). Neglecting H' in Eq. (4), the final total Hamiltonian can be written as

$$\mathsf{H}_T = \sum_i^N \omega_i \mathsf{B}_i^\dagger \mathsf{B}_i + \sum_{i \neq j}^N J_{ij} \mathsf{B}_i^\dagger \mathsf{B}_j + \sum_{i \neq j}^N \frac{K_{ij}}{2} \mathsf{B}_i^\dagger \mathsf{B}_j^\dagger \mathsf{B}_i \mathsf{B}_j$$

$$+ \sum_i^N \frac{\Delta_i}{2} \mathsf{B}_i^\dagger \mathsf{B}_i^\dagger \mathsf{B}_i \mathsf{B}_i - \mathcal{E}(t) \boldsymbol{\mu} \qquad (10)$$

with nonzero coupling elements J_{12}, J_{34}, K_{13}, and K_{24}. Neglecting all nonlinear terms in the dipole expansion [Eq. (5)] we obtain for the coupling to the field

$$\mathcal{E}(t) \boldsymbol{\mu} = \sum_i^N E_i(t)(\mathsf{B}_i^\dagger + \mathsf{B}_i). \qquad (11)$$

For simplicity and easier comparison with NMR results
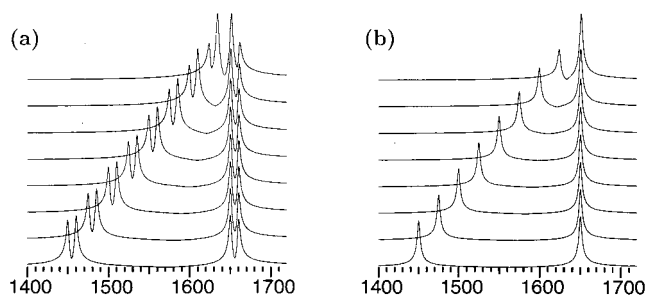
FIG. 6. Dependence of the linear absorption spectra of a system of two coupled chromophores on the relative size of coupling strengths and transition frequency difference. The higher transition frequency is fixed at 1650 cm^{-1} for all spectra while the lower frequency is varied from 1450 cm^{-1} to 1625 cm^{-1} in steps of 25 cm^{-1}. (a) High-temperature initial condition and equal coupling strength ($J = K = 10 \text{ cm}^{-1}$) for diagonal- and off-diagonal coupling (corresponds to NMR). For large transition frequency differences only the splitting due to the diagonal coupling is relevant. (b) Low-temperature initial density matrix and vanishing diagonal coupling. The frequencies are given in cm^{-1}.

where the dipole is the same for all spins of a certain isotope [see Eq. (9)], we use a common dipole matrix element $E_i(t)$ for all chromophores.

The effects of the coupling terms included in our model on NMR and vibrational spectra are most easily illustrated for a pair ($N=2$) of chromophores. In Fig. 6, one-dimensional linear absorption spectra for (a) high- and (b) low-temperature initial condition (compared with the vibrational frequency) are displayed for different coupling situations. The spectra were calculated using sum-over-states expressions.[2] For the linear absorption it is sufficient to consider only the lowest two levels of each chromophore and the initial density matrices can therefore be written in terms of I_z operators. In the high temperature limit we have $\rho_0 = 1 - \sum_i I_{z,i}$ while the low-temperature approximation yields $\rho_0 = \Pi_i(1 - I_{z,i})$. The off-diagonal coupling has a noticeable influence on the spectra only if the transition frequency difference of the chromophores is small or comparable to the coupling strength. This case is called *strong coupling* in NMR and yields a change in line shape known as the *roof effect* [see Fig. 6(a)].[27]

In NMR spectra where the isotropic coupling in the liquid state NMR Hamiltonian contains diagonal as well as off-diagonal couplings with the same coupling strength [see Eq. (8)] the intensity of the peripheral peaks is always reduced with respect to the central lines. For the high-temperature limit of NMR the diagonal coupling yields the splitting of the resonances in multiplets while the intensities in the multiplets depend on the off-diagonal coupling. For weak coupling only the splitting is observed and the off-diagonal coupling can be neglected, which forms the basis of the product operator formalism.[21,27,61] In vibrational systems the two contributions (J and K) can have different strengths, yielding a wider variety of line shapes where, e.g., also the central peaks of a multiplet can have smaller intensities if diagonal and off-diagonal couplings are of different sign. In the low-temperature limit, the diagonal coupling only produces a shift of the peak and no additional splitting. The corresponding spectrum consists only of the lower frequency transitions
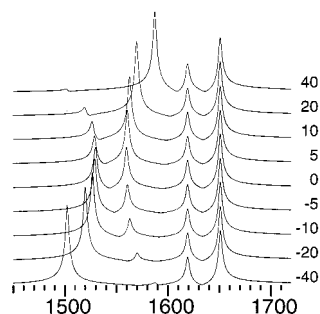
FIG. 7. Dependence of the linear absorption spectrum of the two-band model system [Eq. (10)] with low-temperature initial density matrix on the off-diagonal coupling J_{12} (values given at the right). All other parameters are fixed at the values given in the text. The frequencies and couplings are given in cm^{-1}.

of the NMR multiplets. The influence of the off-diagonal coupling on the line intensities is shown in Fig. 6(b) for vanishing diagonal coupling and positive off-diagonal coupling (H aggregates). For negative off-diagonal coupling (J aggregates) the intensity of the low energy peak increases instead.

The linear absorption spectrum of our four chromophore model system with the parameters given above Eq. (10) is shown in Fig. 7 for different values of J_{12}, as indicated. It is important to note the dependence of the peak intensities of the amide-II band multiplet on the off-diagonal coupling. As discussed previously, no additional splittings due to the diagonal couplings are visible since the initial density matrix is in the low-temperature limit. We have calculated 2D spectra

$$S(\Omega_1,\Omega_2)=\int_0^\infty\int_0^\infty d\tau_1\,d\tau_2\,S(\tau_1,\tau_2)e^{i\Omega_1\tau_1+i\Omega_2\tau_2} \quad (12)$$

for the techniques introduced in Sec. III using the operator propagation expressions of Eq. (26) in Ref. 21 for the time-domain signals $S(\tau_1,\tau_2)$. In the following figures we will always present the absolute value signal $|S(\Omega_1,\Omega_2)|$, if not indicated otherwise. The action of the pulses is expressed in the local oscillator basis while the Greens functions are evaluated in the eigenbasis of the exciton Hamiltonian. The same homogeneous linewidth Γ was assumed for all transitions between the different exciton states. Figure 8 compares a heterodyne detected one-color two-pulse photon echo spectrum [(PE), $-\mathbf{k}_1+\mathbf{k}_2+\mathbf{k}_2'$][44] with the corresponding two-color coherence transfer experiments CT3 (Fig. 2) and CT5 (Fig. 3) with a small homogeneous linewidth of $\Gamma=5$ cm^{-1} for which all peaks are well resolved. The PE spectrum contains the well-known multiplets for the excitonic subsystems[4,62] representing the amide-I [around $(\Omega_1,\Omega_2)=(-1550,1550)$] and amide-II [around $(-1650,1650)$] chromophores, respectively. The excitonic couplings yield intraband cross peaks and the multiplets are asymmetric due to the two-exciton dynamics after the pulse pair. The anharmonicity produces the elongation of the diagonal peaks along Ω_2. The two additional off-diagonal interband multiplets connecting the amide-I and amide-II multiplets around $(-1550, 1650)$ and $(-1650, 1550)$ can be attributed to the diagonal interband couplings K_{ij}.
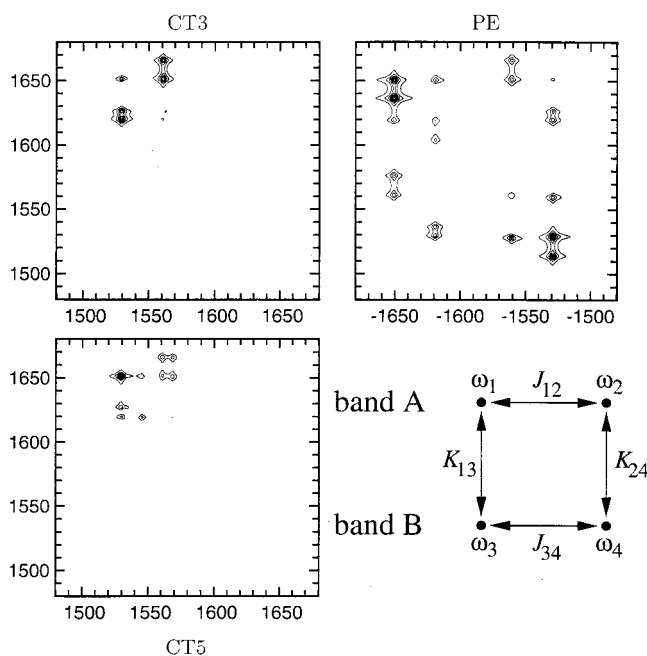
FIG. 8. Comparison of the 2D PE absolute value spectrum for the model system with two dimers with the spectra obtained from the pulse sequences given in Figs. 2 and 3. The values of the couplings and transition frequencies for the model Hamiltonian Eq. (10) are given in the text. Frequencies along the Ω_1 (horizontal) and Ω_2 (vertical) axes are given in cm^{-1}.

The design of the CT3 pulse sequence is based on these coupling terms. The first pulse on the A band produces a single quantum coherence state which evolves at frequencies belonging to A-band chromophores during τ_1. The pulse pair then transfers the coherence to the B band, which leads to an observable signal during τ_2 with B-band frequencies, while the A-band chromophores are in an unobservable population state during τ_2. The CT3 spectrum therefore contains only the interband cross-peak multiplet around (1550, 1650) as can be seen in Fig. 8. The expanded scale display of this cross peak [see Fig. 9(a)] shows that it consists of two doublets due to K_{13} at (1530, 1625) and K_{24} at (1560, 1660) where the splitting in Ω_2 is due to the interband coupling evolution during τ_2. The doublets show an additional cross-
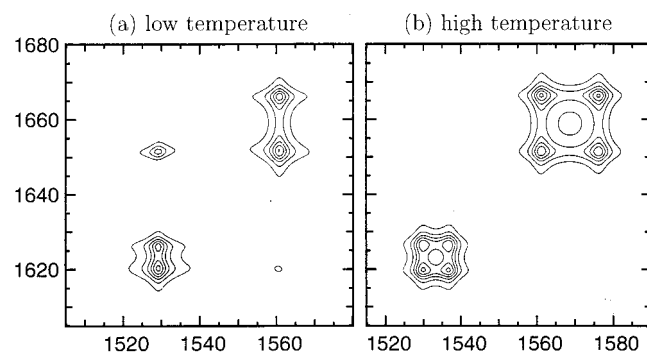
FIG. 9. Enlarged presentation of the interband cross peaks of Fig. 8 obtained with the CT3 technique of Fig. 2 for (a) low- and (b) high-temperature initial condition (see the text). Frequencies along the Ω_1 (horizontal) and Ω_2 (vertical) axes are given in cm^{-1}.
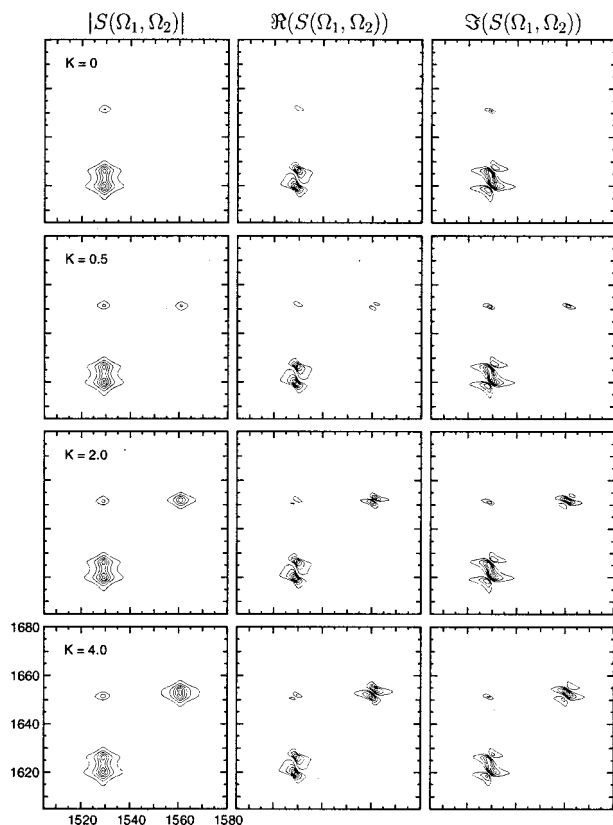
FIG. 10. Dependence of the spectra for the CT3 technique on variations in $K=K_{34}$. All other parameters are fixed at the values given in the text. Frequencies along the Ω_1 (horizontal) and Ω_2 (vertical) axes are given in cm^{-1}.

FIG. 11. The interfering pathways that lead to a cancellation of the interband coupling doublets for vanishing interband coupling K in Figs. 10 (CT3) and 15 (HMQC$'$) are shown for two coupled chromophores. The energy scheme for the system is given at the right and the states are labeled by the number of excitations in each band.

peak pattern at (1530, 1650) due to the resonant coupling J_{ij}. The main difference between NMR and vibrational CT3 signal stems from the different initial conditions. This difference is most apparent in the peak multiplicity along Ω_1 when comparing spectra calculated using low- and high-temperature approximations for the initial density matrix (see Fig. 9). Assuming, again for simplicity, two-level systems, the NMR high temperature approximation yields an initial density matrix of the form $\rho_0 \approx 1 + \Sigma_i I_{z,i}$ while the low-temperature approximation yields $\rho_0 \approx \Pi_i (1 - I_{z,i})$. While ρ_0 in NMR does not contain any two-chromophore correlation of the form $I_{z,i}I_{z,j}$, all of these and all higher order correlations are contained in the low temperature ρ_0. In NMR the two-chromophore correlations such as $I_{z,i}I_{y,j}$ build up between coupled chromophores during τ_1 due to the coupling evolution and τ_1 can be chosen to maximize specific terms. In vibrational spectroscopy all of these terms are already initially present after the first pulse and evolve at their respective frequencies during τ_1. If no cancellation of peaks were present this would in general yield peaks for all possible pairs of chromophores. In practice however only cross peaks between chromophores with a coupling larger than the homogeneous linewidth are observable.

In Fig. 10 the coupling $K_{34}=K$ is varied and the resulting absolute value spectra $|S(\Omega_1,\Omega_2)|$ are shown along the real and imaginary parts of S. The cross-peak signal contains two contributions from different pathways that interfere destructively and cancel if the interband coupling is small com-

pared to the linewidth, as can be seen going from $K=0$ to 4 cm^{-1}. The interference can be most easily understood by considering two coupled chromophores and describing the eigenstates in terms of the approximate local product states. The interfering pathways are shown in Fig. 11 where the first (second) number in the state labels refers to the A-band (B-band) excitation. The contributions have opposite sign as can be seen by counting the number of bra-interactions. For vanishing K the coherences due to the two diagrams evolve with the same frequency during τ_2 which leads to the cancellation. This selectivity greatly simplifies the two-color correlation spectra and yields similar information to that contained in the "shift correlation maps" in NMR spectroscopy using the CT5 scheme.[27] The difference in the initial condition makes the simpler CT3 scheme more valuable for vibrational spectroscopy than in NMR. As mentioned previously, in NMR the π pulse is used to refocus the heteronuclear coupling evolution during τ_1 since the diagonal coupling together with the high-temperature initial condition would yield complicated multiplet patterns in the Ω_1 dimension. For the low-temperature initial condition in vibrational spectroscopy the coupling evolution does not yield multiplets in Ω_1 but only slightly shifted peaks, similar to what can be seen in the linear absorption spectra (see Figs. 7 and 9), and the pulse pair substituting the NMR π pulse is not necessary. The CT5 scheme instead yields more detailed (and more crowded) spectra with additional peaks due to anharmonicities and intraband coupling evolution induced by the pulse pair on the B band. These peaks contain additional information but might not be resolved in realistically broadened spectra, calling for more elaborate pulse sequences.

6812   J. Chem. Phys., Vol. 116, No. 15, 15 April 2002

C. Scheurer and S. Mukamel
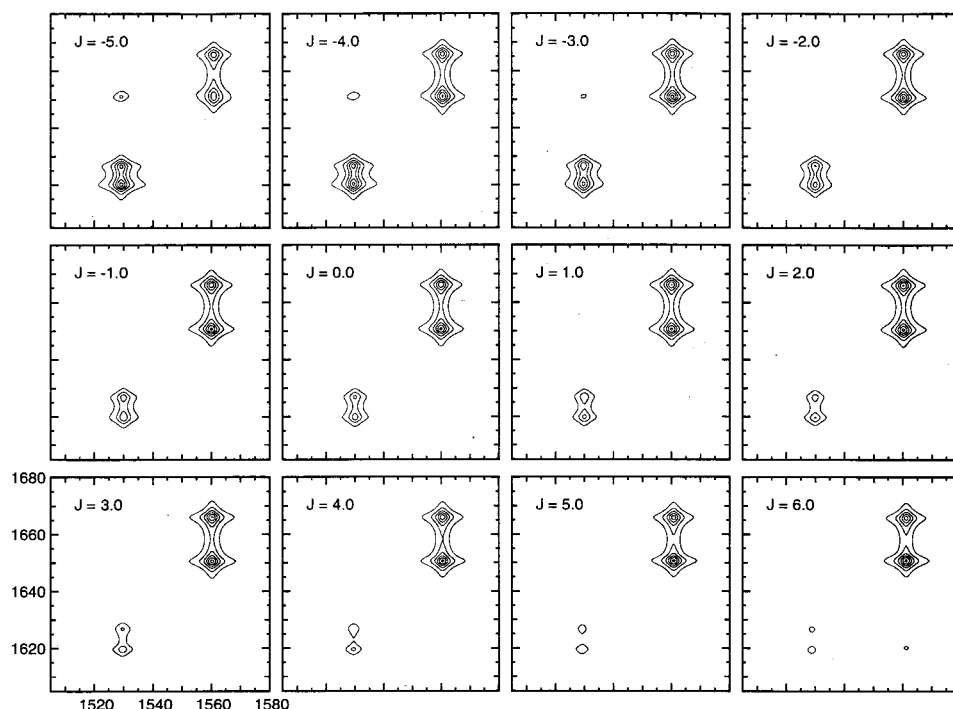
FIG. 12. Dependence of $|S(\Omega_1,\Omega_2)|$ for the CT3 technique on variations in $J=J_{12}$. All other parameters are fixed at the values given in the text. Frequencies along the Ω_1 (horizontal) and Ω_2 (vertical) axes are given in cm^{-1}.

The excitonic off-diagonal couplings J_{ij} influence the relative intensities of the peaks, similar to the linear absorption spectra in Fig. 7. After the initial pulse of the CT3 sequence, the coherences in the system evolve with the same relative weights that also give rise to the linear absorption spectrum. For positive $J=J_{12}$ the coherence between the ground state and the state at $\sim$1530 cm^{-1} becomes weak and thus the doublet at (1530, 1625) in the 2D spectrum disappears (see Fig. 12). The coherence between ground state and the state at $\sim$1560 cm^{-1} becomes stronger and all intensity is transfered to the doublet at (1560, 1660). The intensities in the 2D spectrum can be roughly understood comparing the two linear absorption spectra for $J_{12}=-5$ and $+5$ cm^{-1}. The CT3 experiment correlates single quantum coherences before and after the pulse pair and yields peaks for coherences between chromophores with nonzero interband coupling. The excitation strengths for the individual coherences correspond to the intensities in the linear absorption spectra and the 2D peak intensities are related to the product of these intensities. For $J_{12}=-5$ cm^{-1} the product of intensities of the peaks at 1530 and 1625 cm^{-1} are similar to that of the peaks at 1560 and 1660 cm^{-1} in the linear absorption spectra. Therefore both doublets at (1530, 1625) and (1560, 1660) have about the same strength. For $J_{12}=+5$ cm^{-1} though the product of intensities for the peak at (1530, 1625) is much smaller due to the excitonic coupling and the peak at (1560, 1660) dominates.

Figure 13 displays the vibrational analog of NMR HMQC spectroscopy which shows peaks due to overtones and combination bands in the range from 3150 to 3250 cm^{-1} along Ω_1. After the final (B-band) pulse the system evolves in single quantum states with A-band frequencies during the

detection period τ_2, giving rise to the single quantum frequencies along Ω_2. The detection is restricted to the A band (amide-I) and therefore no peaks below 1600 cm^{-1} are observed in the Ω_2 dimension. As for the CT5 technique, the pulse pair representing the NMR π pulse leads to additional weaker peaks along Ω_1 which are due to intraband couplings, and to the evolution in higher excited states that are shifted by anharmonicity, represented by Δ in the current model. The spectra are simplified considerably when the $\mathbf{k}_3$ pulse pair is eliminated (HMQC$'$) as can be seen in Fig. 14. For the same reason as for the CT3 technique the spectrum contains the double quantum peaks already if $t'=0$ while NMR requires $t'>0$ to generate double quantum states. The spectrum with $t'=0$ actually contains the same peaks as would be observed in a NMR HMQC experiment with ap-
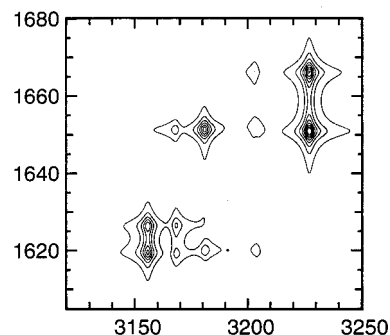
FIG. 13. Vibrational HMQC absolute value spectrum for the model system with two dimers and the pulse sequence given in Fig. 5. The delay time is chosen as $t'=4.2$ ps. Frequencies along the Ω_1 (horizontal) and Ω_2 (vertical) axes are given in cm^{-1}.
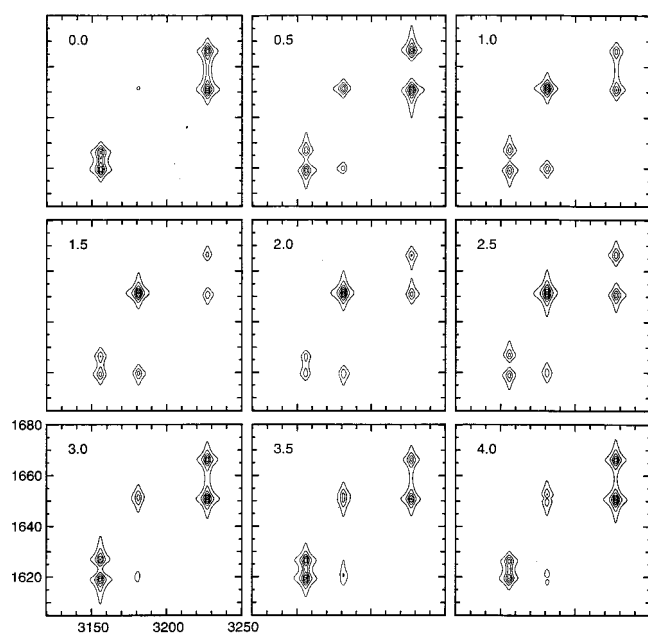
FIG. 14. Dependence of $|S(\Omega_1,\Omega_2)|$ for the HMQC$'$ technique on varia-
tions in $c_0 J t'$ $(J=|J_{12}|=|J_{34}|=5$ cm$^{-1})$, as indicated. Frequencies along
the Ω_1 (horizontal) and Ω_2 (vertical) axes are given in cm^{-1}.

FIG. 15. Dependence of the spectra for the HMQC$'$ technique on variations
in $K=K_{34}$ $(t'=0)$. All other parameters are fixed at the values given in the
text. Frequencies along the Ω_1 (horizontal) and Ω_2 (vertical) axes are given
in cm^{-1}.

propriately chosen t' and no broadband decoupling of the B
band during detection. The double quantum frequencies
along Ω_1 correspond to interband pairs (combination excita-
tions) with nonvanishing couplings while the doublets in Ω_2
correspond to the A-band (amide-I) chromophores involved
in the double quantum states, split by the interband couplings
K_{ij}. The variation of t' (see Fig. 14) yields the additional
double quantum combination peaks at (3180, 1620) and
(3180, 1650) that are not visible for $t'=0$. The cancellation
of pathways for these peaks that are the combinations of the
interband pairs without coupling is lifted by an additional
coherence transfer pathway through the intraband couplings
J_{ij} that are active during t'. This pathway is a close analog
of the coupling evolution used in NMR to generate corre-
lated states through coupling interactions which leads to a
periodic change of the relative peak intensities as shown in
Fig. 14. At $t'=0$ only the doublets at the double quantum
frequencies of the interband coupled chromophores are vis-
ible. For increasing t' their intensities drop and the peaks at
(3180, 1620) and (3180, 1650) become more intense up to a
maximum at about $c_0 J t'=2$ after which the relative intensi-
ties almost go back to their values at $t'=0$.

The selectivity for cross peaks with couplings larger than
the homogeneous linewidth is demonstrated in Fig. 15 and is
completely analogous to the observation for the CT3 scheme.
The Liouville space pathways leading to the cancellation are
given in Fig. 11 for a system of two coupled chromophores.
As can be seen from the energy scheme in Fig. 11, the
HMQC$'$ and the CT3 techniques together allow one to ob-
serve all possible one-quantum coherences in a system of
coupled chromophores if the diagonal coupling term is non-
zero. Variation of the intraband coupling J_{12} leads for t'
$=0$ to the vanishing of the double quantum doublet at (3155,
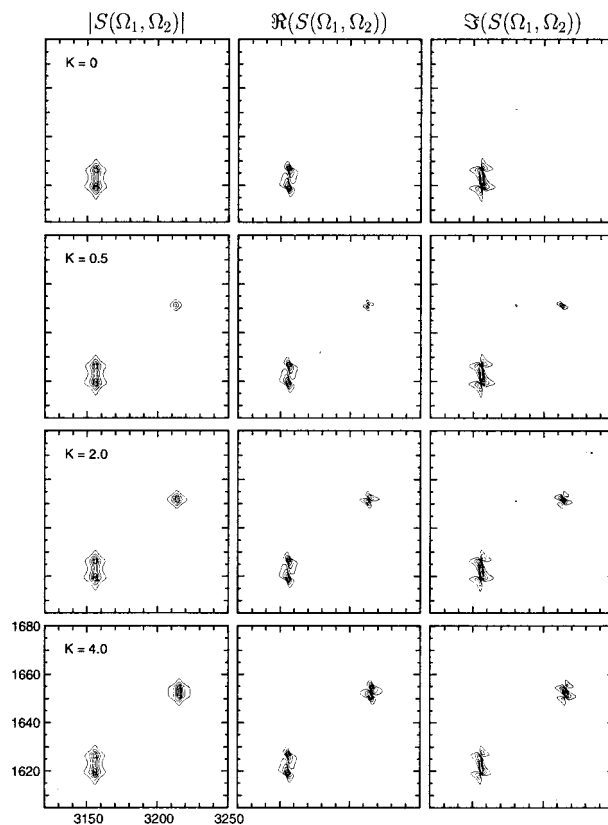
1625) (Fig. 16). This is due to the same reason as discussed
previously for the CT3 sequence only that now the role of
the pulse pair and the single pulse is interchanged. The rela-
tive intensities of the peaks in the 2D spectrum can again be
explained based on the linear absorption spectra for J_{12}
$=-5$ and $+5$ cm^{-1} in Fig. 7. The doublet at (3155, 1625) is
mainly a combination of the transitions at 1530 and 1620
cm^{-1}, which are both weak for $J_{12}=+5$ cm^{-1}. It is thus
much weaker than the doublet at (3180, 1660), which for
$J_{12}=+5$ cm^{-1} is a combination of the two strong transitions
at 1560 and 1620 cm^{-1}. For $J_{12}=-5$ cm^{-1} both doublets
are combinations of one strong and one weak transition each,
yielding peaks of comparable strength. In Fig. 17 a combi-
nation of the behavior of Figs. 14 and 16 is seen for $t'>0$.
For increasing J the doublet at (3155, 1625) becomes weaker
due to the changes in excitation strength already observed in
Fig. 16. On the other hand, the peaks at (3180, 1620) and
(3180, 1650) can build up during the delay t' due to the
coherence transfer through the excitonic coupling. This
mechanism changes the relative intensities of the pathways
in Fig. 11 and lifts the exact cancellation. The peaks with
$\Omega_1=3180$ cm^{-1} are not split along Ω_2 since the states in-
volved in these coherences are only coupled to other states
by off-diagonal coupling terms and these only give rise to
changes in line intensities, not to splittings.
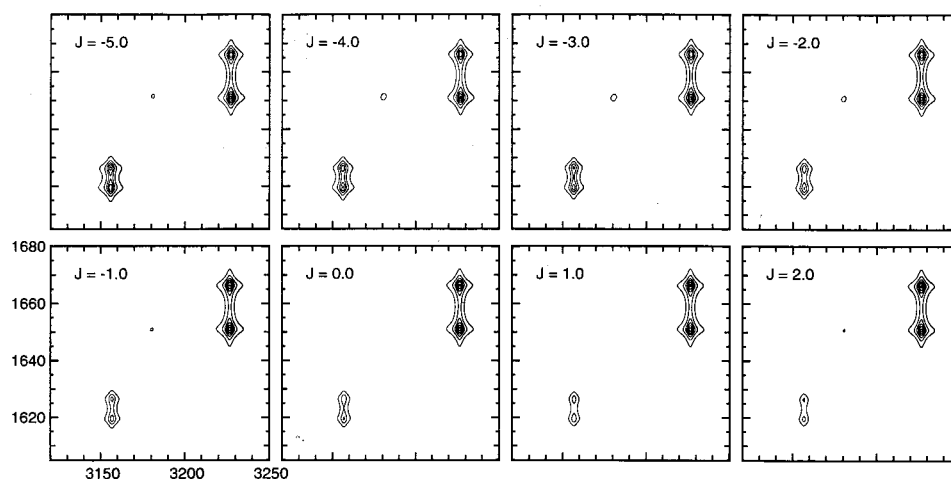
FIG. 16. Dependence of $|S(\Omega_1,\Omega_2)|$ for the HMQC$'$ technique on variations in $J=J_{12}$ ($t'=0$). All other parameters are fixed at the values given in the text. Frequencies along the Ω_1 (horizontal) and Ω_2 (vertical) axes are given in cm^{-1}.

V. CONCLUSIONS

We have surveyed several basic heteronuclear NMR pulse sequences and analyzed them for design principles that may be transferable to vibrational spectroscopy. Heteronuclear NMR spectroscopy corresponds to vibrational spectroscopy of different vibrational bands with pulses that cover individual bands but do not overlap with other bands. We were able to devise a vibrational single quantum experiment that is analogous to the NMR "shift correlation spectroscopy" and a double quantum experiment resembling HMQC. In both cases it is possible to avoid the use of π pulses which are necessary in NMR to simplify the spectra. The different initial conditions of NMR and vibrational spectroscopy (high- versus low-temperature limit) offer different possibilities of selecting specific interband peaks. Time delays used in NMR to create two-chromophore correlated states are not necessary in vibrational spectroscopy where all possible correlated states are already contained in the initial density matrix. Selectivity is achieved through exact cancellation of pathways if no coupling between chromophores exists. These cancellations can be lifted by opening additional pathways using further delay periods as in the case of the HMQC analog (HMQC$'$).

This paper analyzes 2D vibrational techniques that use
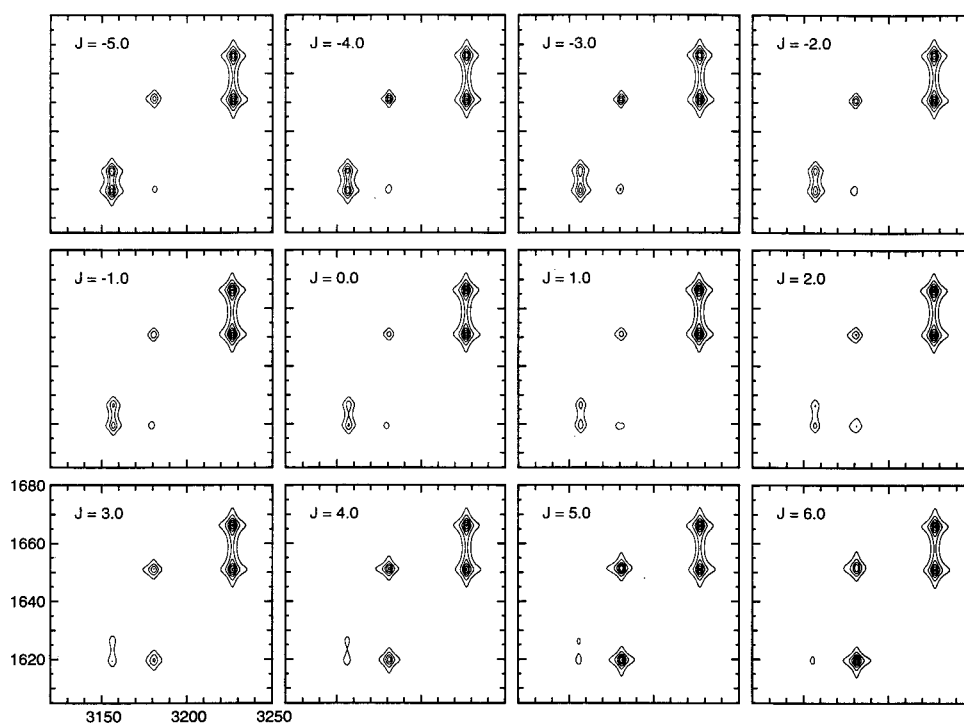
FIG. 17. Dependence of $|S(\Omega_1,\Omega_2)|$ for the HMQC$'$ technique on variations in $J=J_{12}$ ($t'=4.2$ ps). All other parameters are fixed at the values given in the text. Frequencies along the Ω_1 (horizontal) and Ω_2 (vertical) axes are given in cm^{-1}.

different frequencies and are thus analogous to heteronuclear NMR spectroscopy. This should open up a new venue to simplified multidimensional spectra with increased resolution as has been the case in protein NMR spectroscopy. We address the question of which principles can be transferred from NMR spectroscopy and how the spectra and pulse sequences differ from NMR due to the low temperature and weak pulse field limits. To gain this insight we resorted to parameters that allow one to resolve all peaks and make a detailed analysis of the spectra in terms of the coherence transfer pathways possible. The present simulations are thus qualitative since the chosen values of the interband couplings are large and the homogeneous linewidths are small compared to experiment. More realistic simulations of peptide spectra should employ vibrational Hamiltonian that includes more anharmonic contributions needed to describe the interband couplings in multicolor spectroscopies. The influence of relaxation (population relaxation and dephasing) should be introduced as well. The 2D techniques presented in the current paper lay the basis for detailed relaxation studies. In the analogous important NMR experiments, for example, the 2D heteronuclear pulse sequence is used to gain improved resolution and additional delays are introduced and the intensities of certain peaks are monitored as a function of these relaxation delays. Similar ideas may be implemented for the vibrational techniques.

The two three-pulse sequences presented in this paper should be readily implemented experimentally to demonstrate the feasibility of vibrational techniques analogous to heteronuclear NMR spectroscopy. The resulting spectra are far less crowded than third-order one-color experiments. The increased resolution and less overlap will thus allow one to study larger and more complex molecules. The CT3 technique directly yields information about coupled heteropairs of chromophores, their single quantum frequencies in the Ω_1 and Ω_2 dimensions, and the diagonal coupling strengths from the multiplet patterns in Ω_2. HMQC' contains similar information in Ω_2 but yields peaks of the possible combination vibrations along Ω_1. For delays $t' > 0$ between the first two pulses it is additionally possible to extract excitonic coupling patterns and strengths from the additional peaks which have periodically varying intensity as a function of t'. More complicated pulse sequences will have to be developed to gain refined control over the coherence transfer pathways and provide further insight in the dynamics of complex molecules. The use of field polarization and phase provides additional degrees of freedom for coherence control. Effects of relaxation and inhomogeneous broadening will be the subject of future studies.

The present results can be readily extended to multidimensional Raman techniques which might allow one to achieve even higher resolution at the cost of more complicated pulse sequences.[45] To account for the coupling to the field in Raman techniques, the second term in Eq. (4) needs to be replaced with $\mathcal{E}^2(t)\boldsymbol{\alpha}$, where $\boldsymbol{\alpha}$ is the electronic polarizability, averaged over the electronic ground state. The polarizability tensor can be expanded analogously to the dipole in Eq. (5).

[1] A. S. Davydov, *Theory of Molecular Excitons* (Plenum, New York, 1971).
[2] S. Mukamel, *Principles of Nonlinear Optical Spectroscopy* (Oxford University Press, New York, 1995).
[3] S. Mukamel, A. Piryatinski, and V. Chernyak, Acc. Chem. Res. **32**, 145 (1999).
[4] A. Piryatinski, S. Tretiak, V. Chernyak, and S. Mukamel, J. Raman Spectrosc. **31**, 125 (2000).
[5] C. Scheurer, A. Piryatinski, and S. Mukamel, J. Am. Chem. Soc. **123**, 3114 (2001).
[6] S. Mukamel, Annu. Rev. Phys. Chem. **51**, 691 (2000).
[7] M. C. Asplund, M. T. Zanni, and R. M. Hochstrasser, Proc. Natl. Acad. Sci. U.S.A. **97**, 8219 (2000).
[8] R. Zadoyan and V. A. Apkarian, Chem. Phys. Lett. **326**, 1 (2000).
[9] K. A. Merchant, D. E. Thompson, and M. D. Fayer (unpublished).
[10] P. Hamm, M. Lim, W. DeGrado, and R. Hochstrasser, J. Chem. Phys. **112**, 1907 (2000).
[11] K. Okumura, A. Tokmakoff, and Y. Tanimura, J. Chem. Phys. **111**, 492 (1999).
[12] K. D. Rector, A. S. Kwok, C. Ferrante, A. Tokmakoff, C. W. Rella, and M. D. Fayer, J. Chem. Phys. **106**, 10027 (1997).
[13] T. H. Joo, Y. W. Jia, J. Y. Yu, D. M. Jonas, and G. R. Fleming, J. Phys. Chem. **100**, 2399 (1996).
[14] E. J. A. Brown, I. Pastirk, B. I. Grimberg, V. V. Lozovoy, and M. Dantus, J. Chem. Phys. **111**, 3779 (1999).
[15] J. D. Hybl, Y. Christophe, and D. M. Jonas, Chem. Phys. **266**, 295 (2001).
[16] O. Golonzka, M. Khalil, N. Demirdöven, and A. Tokmakoff, Phys. Rev. Lett. **86**, 2154 (2001).
[17] M. Khalil and A. Tokmakoff, Chem. Phys. **266**, 213 (2001).
[18] N. Demirdoven, M. Khalil, O. Golonzka, and A. Tokmakoff, J. Phys. Chem. A **105**, 8025 (2001).
[19] K. A. Merchant, D. E. Thompson, and M. D. Fayer, Phys. Rev. Lett. **86**, 3899 (2001).
[20] D. Keusters, H.-S. Tan, and W. S. Warren, J. Phys. Chem. A **103**, 10369 (1999).
[21] C. Scheurer and S. Mukamel, J. Chem. Phys. **115**, 4989 (2001).
[22] C. Scheurer and S. Mukamel, Bull. Chem. Soc. Jpn. (submitted).
[23] R. R. Ernst, Chimia **29**, 179 (1975).
[24] L. Müller, A. Kumar, and R. R. Ernst, J. Chem. Phys. **63**, 5490 (1975).
[25] W. P. Aue, E. Bartholdi, and R. R. Ernst, J. Chem. Phys. **64**, 2229 (1976).
[26] K. Wüthrich, *NMR of Proteins and Nucleic Acids* (Wiley, New York, 1986).
[27] R. R. Ernst, G. Bodenhausen, and A. Wokaun, *Principles of Nuclear Magnetic Resonance in One and Two Dimensions* (Clarendon, Oxford, 1987).
[28] J. Cavanagh, W. J. Fairbrother, A. G. Palmer III, and N. J. Skelton, *Protein NMR Spectroscopy: Principles and Practice* (Academic, San Diego, 1996).
[29] S. Krimm and J. Bandekar, J. Adv. Protein Chem. **38**, 181 (1986).
[30] *Infrared Spectroscopy of Biomolecules*, edited by H. H. Mantsch and D. Chapman (Wiley–Liss, New York, 1996).
[31] H. Torii, T. Tatsumi, and M. Tasumi, Mikrochim. Acta Suppl. **14**, 531 (1997).
[32] *Protein Folding Special Issue*, edited by J. S. Valentine [Acc. Chem. Res. **31**, 697 (1998)].
[33] H. Torii and M. Tasumi, J. Chem. Phys. **96**, 3379 (1992).
[34] R. B. Dyer, F. Gai, W. H. Woodruff, R. Gilmanshin, and R. H. Callender, Acc. Chem. Res. **31**, 709 (1998).
[35] P. Hamm, M. Lim, W. F. DeGrado, and R. Hochstrasser, Proc. Natl. Acad. Sci. U.S.A. **96**, 2036 (1999).
[36] A. J. Dingley and S. Grzesiek, J. Am. Chem. Soc. **120**, 8293 (1998).
[37] K. Pervushin, A. Ono, C. Fernandez, T. Szyperski, M. Kainosho, and K. Wuthrich, Proc. Natl. Acad. Sci. U.S.A. **95**, 14147 (1998).
[38] F. Cordier and S. Grzesiek, J. Am. Chem. Soc. **121**, 1601 (1999).
[39] G. Cornilescu, J. S. Hu, and A. Bax, J. Am. Chem. Soc. **121**, 2949 (1999).
[40] C. Scheurer and R. Brüschweiler, J. Am. Chem. Soc. **121**, 8661 (1999).

[41] A. J. Dingley, F. Cordier, and S. Grzesiek, Concepts Magn. Reson. **13**, 103 (2001).

[42] C. Scheurer and S. Mukamel (unpublished).

[43] V. Chernyak, W. M. Zhang, and S. Mukamel, J. Chem. Phys. **109**, 9587 (1998).

[44] W. M. Zhang, V. Chernyak, and S. Mukamel, J. Chem. Phys. **110**, 5011 (1999).

[45] A. Piryatinski, V. Chernyak, and S. Mukamel, Chem. Phys. **266**, 311 (2001).

[46] D. L. Clarke and M. A. Collins, J. Chem. Phys. **93**, 7894 (1990).

[47] D. M. Dennison, Rev. Mod. Phys. **12**, 175 (1940).

[48] *J-Aggregates*, edited by T. Kobayashi (World Scientific, Singapore, 1996).

[49] S. Mukamel, S. Tretiak, T. Wagersreiter, and V. Chernyak, Science **277**, 781 (1997).

[50] O. Golonzka and A. Tokmakoff, J. Chem. Phys. **115**, 297 (2001).

[51] R. Hochstrasser, Chem. Phys. **266**, 273 (2001).

[52] M. T. Zanni, N.-H. Ge, Y. S. Kim, and R. Hochstrasser, Proc. Natl. Acad. Sci. U.S.A. **98**, 11265 (2001).

[53] B. Brutscher, Concepts Magn. Reson. **12**, 207 (2000).

[54] G. Lipari and A. Szabo, J. Am. Chem. Soc. **104**, 4546 (1982).

[55] G. Lipari and A. Szabo, J. Am. Chem. Soc. **104**, 4559 (1982).

[56] T. Bremi and R. Brüschweiler, J. Am. Chem. Soc. **119**, 6672 (1997).

[57] S. F. Lienin, T. Bremi, B. Brutscher, R. Brüschweiler, and R. R. Ernst, J. Am. Chem. Soc. **120**, 9870 (1998).

[58] A. Abragram, *The Principles of Nuclear Magnetism* (Clarendon, Oxford, 1961).

[59] C. P. Slichter, *Principles of Magnetic Resonance* (Springer, Berlin, 1990).

[60] P. Hamm, M. Lim, and R. M. Hochstrasser, J. Phys. Chem. B **102**, 6123 (1998).

[61] O. W. Sørensen, Prog. Nucl. Magn. Reson. Spectrosc. **21**, 503 (1989).

[62] P. Hamm, M. Lim, W. F. DeGrado, and R. Hochstrasser, J. Phys. Chem. A **103**, 10049 (1999).